

Self-Assembly and Dynamics Driven by Oligocarbonate–Fluorene End-Functionalized Poly(ethylene glycol) ABA Triblock Copolymers

Guangmin Wei,[⊥] Shrinivas Venkataraman,[†] Yi Yan Yang,[†] James L. Hedrick,^{‡,⊥} and Vivek M. Prabhu^{*,⊥}

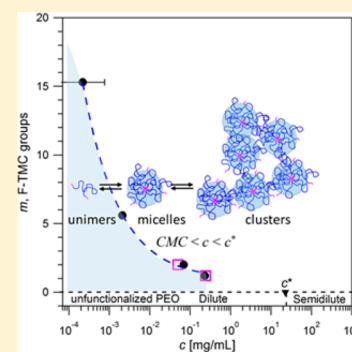
[⊥]Material Measurement Laboratory, National Institute of Standards and Technology, 100 Bureau Drive, Gaithersburg, Maryland 20899, United States

[†]Institute of Bioengineering and Nanotechnology, 31 Biopolis Way, The Nanos, Singapore 138669, Singapore

[‡]IBM Almaden Research Center, 650 Harry Road, San Jose, California 95120, United States

Supporting Information

ABSTRACT: The closed assembly transition from polymers to micelles and open assembly to clusters are induced by supramolecular π – π stacking in model oligocarbonate–fluorene (F-TMC) end-group telechelic polymers. The critical micelle concentration (CMC) depends on the F-TMC degree of polymerization that further controls the weak micelle association and strong clustering of micelles regimes. Clustering follows a multistep equilibria model with average size scaling with concentration reduced by the CMC as $R \sim (c/\text{CMC})^{1/4}$. The F-TMC packing that drives the supramolecular self-assembly from polymers to micelles stabilizes these larger clusters. The clusters are characterized by internal relaxations by dynamic light scattering. This signifies that while F-TMC groups drive the clustering, the micelles interconnected via F-TMC bridging interactions remain coupled to the extent that the clusters relax via Rouse–Zimm dynamics, reminiscent of microgels.



INTRODUCTION

Polymeric micelles self-assembled from amphiphilic block copolymers are employed in aqueous media as nanocarriers for hydrophobic drugs with high loading capacity and physical stability.^{1–3} The hydrophobic core provides a reservoir for encapsulation of water-insoluble therapeutics, and the hydrophilic shell ensures dispersion in aqueous media. As new functional groups are incorporated, different micellar morphologies are observed due to the interplay of driving forces including electrostatic assembly,⁴ hydrogen bonding,⁵ π – π stacking interactions,^{6–8} liquid crystalline packing,^{9,10} and crystallization.^{11,12}

Agrawal et al.¹¹ performed small-angle neutron scattering (SANS) to understand the self-assembly of poly(lactide)–poly(ethylene oxide)–poly(lactide) (PLA–PEO–PLA) in aqueous solutions and gels as a function of block length and stereochemistry of PLA. They found that D/L-lactic acid blocks form amorphous, spherical core micelles, whereas polymers with L-lactic acid blocks form crystalline, lamellar micelles. In this case, the molecular packing within the micellar core provides flexibility when designing advanced materials.¹³ In another example, strongly associating cholesterol-functionalized PEO triblock copolymers form versatile gels through the supramolecular assembly of disk-like micelles,¹⁴ where smectic order appears in related cholesterol-functionalized diblock system.¹⁰ The micelle structure, local chain conformation, and connectivity of micelles through bridging will determine the transient network necessary for thermoreversible rheological properties of injectable gels.^{15,16}

The interplay between micellization and clustering in systems with anisotropic and strong interactions may be differentiated from polyoxyalkylenes. Poly(oxybutylene)–poly(oxyethylene)–poly(oxybutylene) ($B_mE_nB_m$)^{17–22} displays unimer to flower-like micelle structure in dilute solution with critical micelle concentration determined by the insoluble block length.²⁰ The solution aggregation of micelles was observed by SANS,¹⁹ but not as a function of concentration and end-block length.²⁰ A related system, poly(oxypropylene)–poly(oxyethylene)–poly(oxypropylene) ($P_mE_nP_m$), did not show micellization²³ at room temperature but did show micellization and clustering at elevated temperature.²⁴ Similarly, $E_nP_mE_n$ exhibits a drug-loading-dependent micellization.²⁵ Interestingly, even PEO exhibits clustering.^{26,27} The molecular origins of this clustering were modeled by considering PEO as a copolymer composed of hydrophilic ether and hydrophobic ethylene groups. Hammouda devised a copolymer theory to quantify the clustering from SANS.²⁸ However, clustering also depends upon the specific PEO end groups.²⁷ Therefore, clustering properties in ABA block copolymers and telechelic polymers may have multiple origins, inherent in the main chain, as well as enhanced by the end-group functionality.

We provide a systematic study of model aqueous solutions of oligocarbonate–fluorene (F-TMC) end-functionalized poly(ethylene glycol) triblock copolymer, $P(\text{F-TMC})_m\text{-P(EG)}_n\text{-}$

Received: November 22, 2016

Revised: January 19, 2017

Published: February 3, 2017

Table 1. Polymer Characteristics of $F_mE_{445}F_m$ Triblock Copolymer Studied

sample	$F_mE_nF_m$	PEG M_n^a (g/mol)	n , PEG ^b	m , F-TMC ^c	polymer M_w^d (g/mol)	$(dn/dc)^e$ (cm ³ /g)
ABA-F1	$F_{15.3}E_{445}F_{15.3}$	19610	445	15.3	27247	0.148 ± 0.002
ABA-F2	$F_{5.6}E_{445}F_{5.6}$	19610	445	5.6	22358	0.126 ± 0.004
ABA-F3	$F_2E_{445}F_2$	19610	445	2.0	20544	0.1355 ± 0.0006
ABA-F4	$F_{1.2}E_{445}F_{1.2}$	19610	445	1.2	20141	0.1371 ± 0.0002

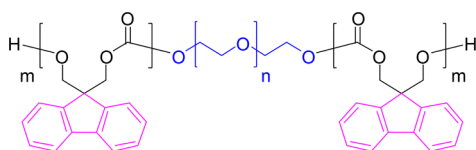
^aNumber-average molecular mass data based on hydroxyl value from supplier. ^bCalculated from the supplier data. ^cBased on ¹H NMR spectroscopy. ^d $M_w^e = M_n^{PEG} + 2m \times M_n^{F-TMC}$. ^eRefractive index increment with 18 MΩ-cm resistivity water.

$P(F-TMC)_m$. In these systems, the driving force for association is due to π - π stacking interactions that induce micelle formation²⁹ not formed in PEO.³⁰ It is shown that the closed assembly formation common to micelles occurs in the presence of enhanced clustering driven by F-TMC. The concentration dependence of the cluster formation is compared to mean-field predictions.

EXPERIMENTAL METHODS^A

We refer to the series in the following manner $F_mE_nF_m$ to represent $P(F-TMC)_m$ - $P(EG)_n$ - $P(F-TMC)_m$ as shown in Scheme 1. E represents the middle poly(ethylene glycol), and F is the symmetric substituted oligocarbonate fluorene group with degree of polymerizations n and m , respectively. This avoids confusion from prior notation of the series as ABA-F1, ABA-F2, ABA-F3, and ABA-F4. These notations are provided in Table 1 for cross-consistency with previous work^{29,31} along with polymer characteristics. These polymers, with the hydrophobic group number $m = 15.3, 5.6, 2.0$, and 1.2 , are named as $F_{15.3}E_{445}F_{15.3}$, $F_{5.6}E_{445}F_{5.6}$, $F_2E_{445}F_2$, and $F_{1.2}E_{445}F_{1.2}$, respectively. The selective solvent used in this study is 18 MΩ-cm resistivity water.

Scheme 1. Chemical Structure of $F_mE_{445}F_m$ Triblock Copolymer



Sample Preparation. $F_{15.3}E_{445}F_{15.3}$ and $F_{5.6}E_{445}F_{5.6}$ block copolymers (2.0 mg) were dissolved in 2.0 mL of inhibitor-free tetrahydrofuran in a clean glass vial and stirred for ≈ 2 h. These clear polymer solutions were transferred to a prewashed dialysis membrane with molecular mass cutoff of 3500 Da and dialyzed at room temperature against water (1 L) that was changed after 3, 18, and 21 h. Typically, the final concentration of the polymer solution after dialysis was 0.6 mg/mL, which could form some sediment. These $F_{15.3}E_{445}F_{15.3}$ and $F_{5.6}E_{445}F_{5.6}$ solutions were vortexed and then serially diluted. The final concentration was between 1.5×10^{-3} and 0.5 mg/mL. Sample $F_{5.6}E_{445}F_{5.6}$ was filtered by 0.45 μ m PVDF membrane, whereas $F_{15.3}E_{445}F_{15.3}$ were not filtered. $F_2E_{445}F_2$ and $F_{1.2}E_{445}F_{1.2}$ block copolymers were dissolved directly in water as clear solutions of 10 mg/mL with stirring. After approximately 24 h, the solutions were diluted to the required concentrations 0.13–10 mg/mL, and each solution was filtered by 0.45 μ m PVDF membrane before light scattering experiments.

Ultraviolet–Visible (UV–Vis) Spectroscopy. UV–vis spectra were measured by a PerkinElmer UV WinLab spectrophotometer in the spectral range of 180–600 nm in water using quartz cuvettes of 10 mm path length at room temperature. The polymer concentration was 0.01 mg/mL. The absorption spectrum of water was used as baseline and subtracted correspondingly.

dn/dc Measurement. The refractive index increment, dn/dc , of $F_mE_{445}F_m$ in 18 MΩ-cm resistivity water was measured by a Wyatt Optilab rEX at 685 nm using a flow rate of 0.5 mL/min and provided

in Table 1. Five concentrations spanning 10–0.625 mg/mL were used for $F_2E_{445}F_2$ and $F_{1.2}E_{445}F_{1.2}$. Similarly, 0.80–0.04 mg/mL was used for the remaining. The larger dn/dc value for $F_{15.3}E_{445}F_{15.3}$ may be related to a higher packing density of F-TMC within the dispersion, but we were unable to independently verify this.

Laser Light Scattering. Static and dynamic laser light scattering measurements were performed with a modified Brookhaven BI-200SM using a wavelength of 532 nm laser light from a Coherent VERDI diode-pumped solid state laser operating in TEM₀₀ mode. Glan-laser polarizer and analyzer (Thorlabs) were used under the vertical polarizer and vertical analyzer condition for all experiments for samples thermostatically controlled to 25.0 °C by a recirculating bath to control the temperature of the decalin index matching bath. The laser power was finely adjusted by neutral density filters. A pinhole before the photomultiplier tube detector was adjusted for static (1 mm) or dynamic (100 μ m) light scattering. The intensity was corrected for reflection, scattering volume variation with angle, and refraction by standard methods. The excess scattering above the solvent level was placed onto Rayleigh ratio units using toluene as a reference.^{32,33}

In static polarized laser light scattering the excess Rayleigh ratio, $R_{vv}(c,q)$, is measured as a function of scattering wave vector (q), where $q = (4\pi n/\lambda) \sin(\theta/2)$ and θ is the scattering angle. $R_{vv}(c,q)$ from dilute polymer solutions is related to the mass-average molecular mass, M_w , by³⁴

$$\frac{Hc}{R_{vv}(c,q)} = \frac{1}{M_w P(q)} + 2A_2c + 3A_3c^2 + \dots \quad (1)$$

where c is the polymer concentration. The optical constant, $H = 4\pi^2 n^2 (dn/dc)^2 / \lambda^4 N_A$, combines the solvent refractive index (n), refractive index increment (dn/dc), wavelength of light (λ) in a vacuum, and Avogadro's number (N_A). The concentration dependence of the excess scattering estimates the second and third virial coefficients, A_2 and A_3 , respectively. The form factor, $P(q)$, measures the characteristic particle size and shape from the angular dependence of the scattered light. When $qR_g < 1$, where R_g is the polymer radius of gyration, the particle form factor has the following form:

$$\frac{1}{P(q)} = 1 + \frac{q^2 \langle R_g^2 \rangle}{3} + \dots \quad (2)$$

A Zimm plot of $Hc/R_{vv}(c,q)$ against $q^2 + kc$, with k being a scaling constant, results into the two limiting lines $Hc/R_{vv}(c=0,q)$ and $Hc/R_{vv}(c,q=0)$; the first yields $1/M_w + P(q)$, and the latter gives $1/M_w + 2A_2c + 3A_3c^2 + \dots$ where $q=0$ is obtained by extrapolation.³⁵ These double extrapolations to obtain M_w , R_g , and A_2 are not always simple if curvature appears in $Hc/R_{vv}(c,q)$. In these cases, a Berry plot was used, where the square root of $Hc/R_{vv}(c,q)$ is plotted versus $q^2 + kc$.³⁶ This method was applied recently to characterize block copolymer vesicles.³⁷

Dynamic laser light scattering (DLS) measures the intensity–intensity time correlation function $g^{(2)}(q,\tau)$ by means of a multi-channel digital correlator and related to the normalized electric field correlation function $g^{(1)}(q,\tau)$ through the Siegert relation.³⁸ Herein, two different procedures were used to analyze $g^{(1)}(q,\tau)$. For $F_{1.2}E_{445}F_{1.2}$ and $F_2E_{445}F_2$ at higher polymer concentration, two modes were confirmed by the inverse Laplace transform method of CONTIN.³⁹ In the presence of two modes and in order to facilitate comparison to a

theory, $g^{(1)}(q, \tau)$ was fit by a sum of a single exponential and a stretched exponential function

$$g^{(1)}(q, \tau) = a_1 \exp(-\Gamma_1 \tau) + a_2 \exp(-[\Gamma_2 \tau]^\beta) \quad (3)$$

where a_i and Γ_i are the amplitude and characteristic decay rate of the i mode, respectively, and β is a stretched exponent. The translational diffusion coefficient is obtained from $D_i = \Gamma_i/q^2$. For $F_{1,2}E_{445}F_{1,2}$ and $F_2E_{445}F_2$ at very low polymer concentration, as well as $F_{5,6}E_{445}F_{5,6}$ and $F_{15,3}E_{445}F_{15,3}$ in the entire polymer concentration range, only one mode was observed by CONTIN. In this case, the quadratic cumulant method⁴⁰ was used to evaluate $g^{(1)}(q, \tau)$ to estimate the average diffusion coefficient ($D = \bar{\Gamma}/q^2$) from the mean decay rate $\bar{\Gamma}$, and size polydispersity ($\mu_2/\bar{\Gamma}^2$). The hydrodynamic radius R_h was estimated using the Stokes–Einstein relation, where $R_h = k_B T/6\pi\eta_0 D$ with known Boltzmann constant (k_B), solvent viscosity (η_0), and temperature (T).

Uncertainties (error bars) are estimated by one standard deviation from the mean by fits to static light scattering and DLS data by least-squares minimization. While error bars are shown, they may be smaller than the symbols.

RESULTS AND DISCUSSION

Molecular Association of F-TMC Groups. The UV–vis spectrum provides direct evidence for π – π stacking of F-TMC groups. The F-TMC monomer has an absorption peak at 257 nm in chloroform.⁴¹ When F-TMC groups associate, the UV–vis spectrum may show a red-shift of the primary absorption peak^{42,43} as well as introduction of multiple peaks due to J- or H-coupling.⁴⁴ The red-shifted peak shows that the side-chain fluorene groups are stacked close enough to cause π – π interaction in the ground state.^{42,43} In Figure 1, the absorption

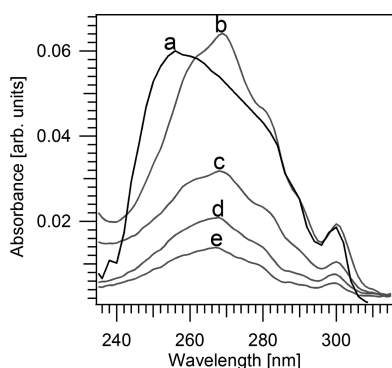


Figure 1. UV–vis absorption spectra of F-TMC monomer (a) in chloroform and of $F_{15,3}E_{445}F_{15,3}$ to $F_{1,2}E_{445}F_{1,2}$ (b–e) in water. The data of F-TMC monomer in chloroform are taken from ref 41. The concentration of $F_{15,3}E_{445}F_{15,3}$ to $F_{1,2}E_{445}F_{1,2}$ in water is 0.01 mg/mL.

spectra of $F_{15,3}E_{445}F_{15,3}$ to $F_{1,2}E_{445}F_{1,2}$ in water have significant red-shifts compared to the F-TMC monomers in chloroform, demonstrating that the side chain fluorene groups have π – π stacking interaction between each other in self-assembled structures.

Critical Micelle Concentration. $Hc/R_w(c, q = 0)$ provides the mass-average molecular mass and virial coefficient through eq 1. The $F_m E_{445} F_m$ polymers display a sharp decrease in $Hc/R_w(c, q = 0)$ with increasing concentration followed by a small positive or negative slope. This concentration dependence of $Hc/R_w(c, q = 0)$, shown in Figure 2, occurs far below the chain overlap concentration, $c^* = 3M_{n,PEG}/4\pi R_{g,PEG}^3 N_A \approx 24$ mg/mL. While the slope at higher concentration may be described by eq 1, the appearance of the upturn at very low concentration follows systems that exhibit a critical micelle concentration

(CMC).^{45–49} Methods to quantify the CMC by light scattering may differ. For instance, Harada et al.⁴⁹ used the intersection of two lines between a low and high concentrations regime to define the critical association concentration in order to distinguish it from the CMC as determined by fluorescence methods. Nolan et al.⁴⁸ modified the Debye equation (eq 1) and applied it to a well-defined self-assembling polymer system into the following form

$$\frac{Hc}{R_w(q = 0)} = \frac{1}{M_w^s c_s + M_w^{mic} \frac{(c - c_s)}{c}} + 2A_2 c + 15/8 A_2^2 M_w^{mic} c^2 \quad (4)$$

where c is the total polymer concentration and c_s is the concentration of unassociated polymer (unimer). The details may be found in Nolan et al.,⁴⁸ but briefly the first term on the right is obtained by expanding the mass-average molecular mass, M_w , into a component due to the unimer, M_w^s , and micelle, M_w^{mic} . The second and third terms are contributions from the second and estimated third virial coefficient. Equation 4 was fit to each data set in Figure 2 with fit parameters c_s , M_w^{mic} , and A_2 .

Far below the CMC, the polymers are unassociated with concentration of unimer equals to that of the polymer. Above the CMC, micelles form, and the concentration of micelles is $c - c_s$. For a monodisperse block copolymer, c_s remains constant for c greater than the CMC. However, for polydisperse block copolymers, c_s may increase above the CMC.⁵⁰ In either case, the contribution of micelles causes Hc/R_w to decrease with polymer concentration. Considering that the CMC is effectively the concentration at which the presence of micelles is just detectable by static light scattering, the CMC can be taken as the point below which the inverse molecular mass remains constant.⁵¹ We assign c_s as CMC, using the simplifying assumption that the concentration of unassociated polymers remains constant above the CMC.

The CMC obtained from c_s is shown as the filled circles (●) in Figure 3. These data are in quantitative agreement with the CMC determined by a pyrene fluorescence-quenching method for $F_2E_{445}F_2$ and $F_{1,2}E_{445}F_{1,2}$ shown as the open squares (□), confirming the applicability of eq 4. The CMC values successively decrease with increasing F-TMC group number (m) as summarized in Table 2.

The free energy of micellization for a monodisperse block copolymer is given by $\Delta G^{\circ}(\text{mic}) = (N_A k_B) T \ln \text{CMC}$.⁵⁰ For alkylene surfactants, $\Delta G^{\circ}(\text{mic})$ is proportional to the number of methylene groups (N) and generally follows $\log \text{CMC} = a'N + b'$, where a' and b' are constants.⁵² However, block copolymers deviate from this expression due to the interfacial energy associated with chain packing at the core and corona interface.^{50,53,54} Classical predictions⁵⁵ find $\log \text{CMC} \sim N^{2/3}$. Fits to the CMC data (Figure 3) find $\log \text{CMC} = (-1.77 \pm 0.43)m^{0.47 \pm 0.08} + (1.29 \pm 0.045)$, which falls between limits^{50,55} observed by polymeric micelles of $N^{1/3}$ and $N^{2/3}$.

Identifying Weakly Associating Micelles and Strong Clustering Regimes. In dilute solutions ($c \approx \text{CMC}$), when excess light scattering was just detectable, only one mode was observed by DLS. For $F_2E_{445}F_2$ and $F_{1,2}E_{445}F_{1,2}$ at higher concentrations two well-separated modes were observed. In this case, established methods were applied to separate the excess light scattered intensity into two populations from the DLS relative amplitudes a_1 (fast mode) and a_2 (slow mode).³⁸ These two populations at $c > \text{CMC}$ are due to the presence of micelles, $I_1(q) = a_1(q)R_w(q)$, and clusters, $I_2(q) = a_2(q)R_w(q)$,

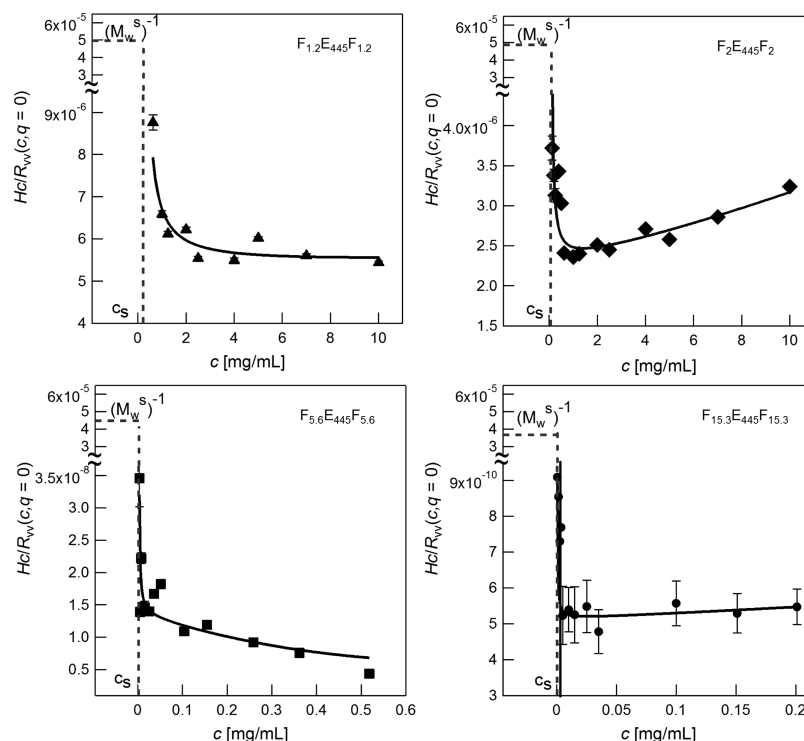


Figure 2. Reduced scattered intensity $Hc/R_w(c, q = 0)$ versus polymer concentration for $F_{15.3}E_{445}F_{15.3}$ to $F_{1.2}E_{445}F_{1.2}$. $R_w(c, q = 0)$ is the Rayleigh ratio extrapolated to $\theta = 0^\circ$. Note the break in the y -axis. Solid lines are fits of eq 4 with fixed molecular mass of unimer, M_w^* . The dashed line notes the fit values of c_s . The inverse of molecular mass is depicted as $Hc/R_w(c, q = 0)$.

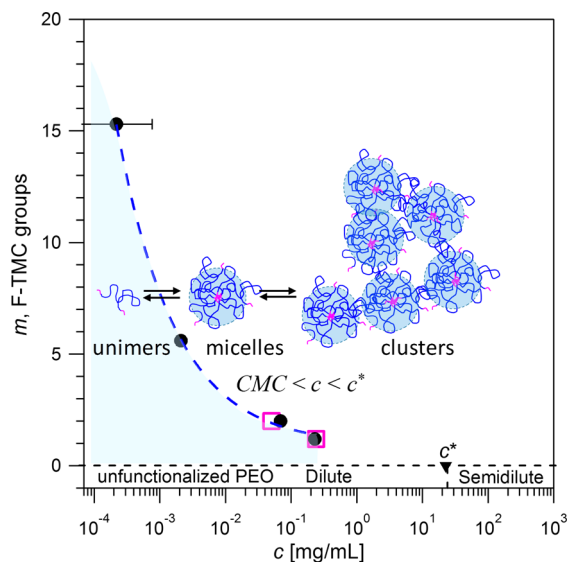


Figure 3. State diagram in the F-TMC group number (m)–polymer concentration (c) plane at a fixed temperature $T = 25^\circ\text{C}$. Filled circles (●) represent the CMC obtained from eq 4. Open squares (○) represent the CMC by fluorescence quenching from ref 29. The overlap concentration (c^*) of the unassociated PEG is shown.

as initially communicated.³¹ Figure 4 shows two regimes in the evolution of the reduced scattered intensities versus c/CMC . The shaded region represents a weak micelle association regime followed by a strong clustering regime distinguished by the presence of micelles and clusters of micelles. The weak micelle association and strong clustering regimes occur within the diagram of Figure 3 as will be discussed.

The second virial coefficient obtained by the Zimm plots for $F_2E_{445}F_2$ and $F_{1.2}E_{445}F_{1.2}$ and Berry plots for $F_{5.6}E_{445}F_{5.6}$ and $F_{15.3}E_{445}F_{15.3}$ within the strong clustering regime are provided in Table 2. A_2 is smaller than the parent polymer (PEG of $M_w = 19\,610\text{ g/mol}$), which is on the order of $10^{-3}\text{ mol}\cdot\text{cm}^3/\text{g}^2$.⁵⁶ Smaller A_2 values for the series $F_{15.3}E_{445}F_{15.3}$ to $F_{1.2}E_{445}F_{1.2}$ in comparison to the unfunctionalized homopolymer are consistent with the formation of polymeric micelles and aggregation.⁵⁷ The very small and negative A_2 implies weak attraction between clusters. From positive A_2 , we can reliably estimate the cluster overlap concentration by $c^* = 1/(A_2M_w)$ for $F_2E_{445}F_2$, leading to $c^* = 35\text{ mg/mL}$.⁵⁸

The mass-averaged molecular mass shown in Table 2 are in agreement with those determined by eq 4 (Table S1). For $F_2E_{445}F_2$ and $F_{1.2}E_{445}F_{1.2}$, the aggregation number, N_{agg} , calculated from the extrapolated M_w , corresponds well to the aggregation number of micelles and is consistent with previous estimates.²⁹ For $F_{15.3}E_{445}F_{15.3}$ and $F_{5.6}E_{445}F_{5.6}$ the value of N_{agg} is too high for isolated micelles. We will show that the high N_{agg} of $F_{15.3}E_{445}F_{15.3}$ and $F_{5.6}E_{445}F_{5.6}$ is due to kinetically frustrated clusters without clear separation into free micelles by DLS.

Concentration Dependence of the Radius of Gyration of Clusters. In the strong clustering regime, $\langle R_g \rangle$ was estimated from $I_2(q)$ (Figure S2) by⁵⁹

$$\langle R_g^2(c) \rangle = 3 \frac{d}{dq^2} \left[\frac{Hc}{I_2(q, c)} \right]_{c/} \bigg/ \left[\frac{Hc}{I_2(q, c)} \right]_{q=0, c=0} \quad (5)$$

In the case of $F_{15.3}E_{445}F_{15.3}$ and $F_{5.6}E_{445}F_{5.6}$, $\langle R_g \rangle$ was estimated from $[R_w(q)]^{1/2}$ (Figure S3). Figure 5 shows the apparent $\langle R_g \rangle$ as a function of c/CMC within the strong clustering regime. While all the data do not collapse onto a single master curve, when normalized by the CMC, the scaling is compared to a $1/4$

Table 2. Parameters from Static Laser Light Scattering of $F_mE_{445}F_m$ Triblock Copolymer

$F_mE_nF_m$	CMC (mg/mL)	M_w (g/mol)	A_2 (mol·cm ³ /g ²)	N_{agg}^e	R_g (nm)
$F_{15.3}E_{445}F_{15.3}$	0.000216 ± 0.000442^a	$(1.34 \pm 0.25) \times 10^9^c$	$(-7.38 \pm 0.65) \times 10^{-8}^c$	49180^c	226 ± 1^c
$F_{5.6}E_{445}F_{5.6}$	0.0021 ± 0.0003^a	$(6.99 \pm 0.36) \times 10^7^c$	$(-1.30 \pm 0.16) \times 10^{-5}^c$	3126^c	94 ± 1^c
$F_2E_{445}F_2$	0.069 ± 0.002^a	$(4.51 \pm 0.25) \times 10^5^d$	$(6.41 \pm 1.58) \times 10^{-5}^d$	22 ± 1.2^d	36 ± 2^d
	0.050^b				
$F_{1.2}E_{445}F_{1.2}$	0.231 ± 0.011^a	$(1.77 \pm 0.08) \times 10^5^d$	$(2.15 \pm 24.0) \times 10^{-7}^d$	9 ± 0.4^d	39 ± 1^d
	0.240^b				

^aCMC obtained from eq 4. ^bCMC by pyrene fluorescence-quenching method.²⁹ ^cBerry plot from R_{wv} (Figure S1). ^dZimm plot from $I_2(q)$ (Figure S1). ^e $N_{agg} = M_w/M_w^s$ using M_w^s from Table 1.

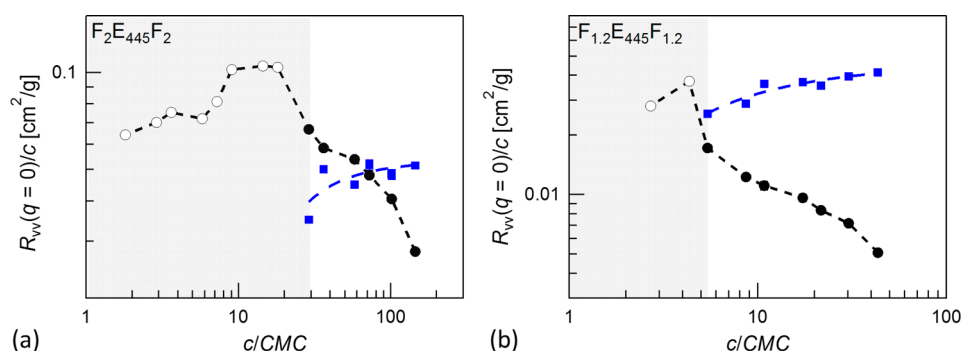


Figure 4. Concentration-normalized extrapolated intensity versus reduced concentration obtained from Zimm plots. The gray shaded region highlights a regime of weakly associating micelles (○) that transitions to strong micelle clustering with populations of micelle ($I_1(q)$, ●) and clusters ($I_2(q)$, ■).

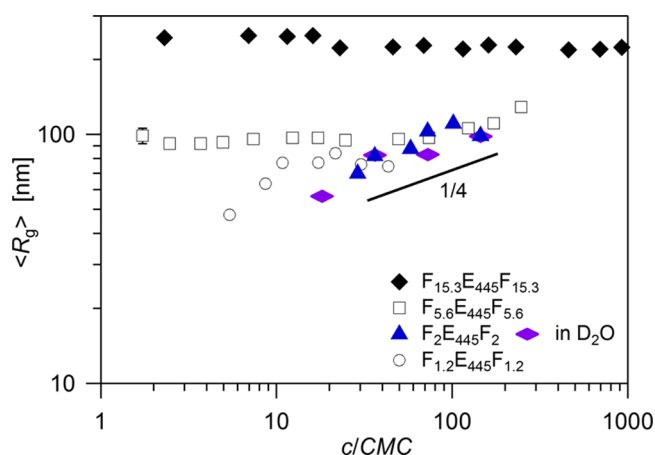


Figure 5. Normalized concentration dependence of the apparent radius of gyration of clusters ($\langle R_g \rangle$) for $F_{15.3}E_{445}$ to $F_{1.2}E_{445}F_{1.2}$ as indicated in the legend including data in D_2O from ref 31.

power law. The onset of the strong clustering regime occurs at smaller c/CMC for $m = 1.2$, when compared to $m = 2$ in Figure 4 and also observed by $\langle R_g \rangle$ in Figure 5. At higher m the value of the segregation strength $\chi_{AS}m$ increases, where χ_{AS} is the Flory–Huggins interaction parameter between F-TMC and water. Therefore, the segregation strength and selective solubility of the end groups increase with m , further increasing the driving force for partitioning of F-TMC into micelles. If F-TMC groups are buried into flower-like micelles, then the probability of the end group is strongly localized into a central core with reduced probability to the micelle periphery. The probability of micelle-to-micelle contact increases with c^2 , regardless of $\chi_{AS}m$, but the probability of end groups fluctuating from core to solution should decrease with increasing $\chi_{AS}m$. This trend overall shifts the expected cluster growth

concentration dependence to higher c/CMC . The lattice simulations by Nguyen-Misra and Mattice demonstrate that the loop fraction increases and dangling end fraction decreases as polymer concentration increases or solvent-end group compatibility decreases.⁶⁰ Further, the fraction of loops also depends upon the middle block stiffness with flexible chains exhibiting only 0.25 fraction of loops in a molecular dynamics study of strongly associating telechelic polymers.⁶¹ So, the true situation of all loop-like micelles is not expected, but a combination of loops and dangling or bridging chains ends that facilitates cluster formation.

Dynamics of Micelles and Clusters. The angular dependence of dynamic laser light scattering provides insight into the F-TMC degree of polymerization and polymer concentration dependence within the weakly associating micelle and strong clustering regimes. For $F_{15.3}E_{445}F_{15.3}$ and $F_{5.6}E_{445}F_{5.6}$ the normalized DLS spectrum observe one broad mode as shown for one concentration in Figures 6a and 6b (lower inset). The diffusion coefficient ($D = \bar{\Gamma}/q^2$) in the upper inset shows a plateau with a positive deviation to higher q in the case of $F_{5.6}E_{445}F_{5.6}$. This deviation is also observed in the lower m systems and contains intracluster dynamics information.⁶²

Typical normalized DLS for $F_{1.2}E_{445}F_{1.2}$ and $F_2E_{445}F_2$ are shown for one concentration in Figure 7a,b. Within the strong clustering regime as shown in Figure 7, the micelle diffusion coefficient was determined from $D_1 = \Gamma_1/q^2$, while the cluster effective diffusion coefficient $D_2 = \Gamma_2/q^2$ determined from the low q region. Systematic positive deviation in D_2 is shown in the upper insets. This is attributed to concentration fluctuations within clusters.^{31,63} Such behavior was recently observed in supramolecular assembled fibers.⁸ An example of the separated scattered intensities by the cluster and micelle are provided in the lower inset. $I_2(q)$ exhibits a q -dependence, fit by eq 2, whereas $I_1(q)$ typically did not display a systematic q -dependence, and estimates to obtain the free micelle R_g are

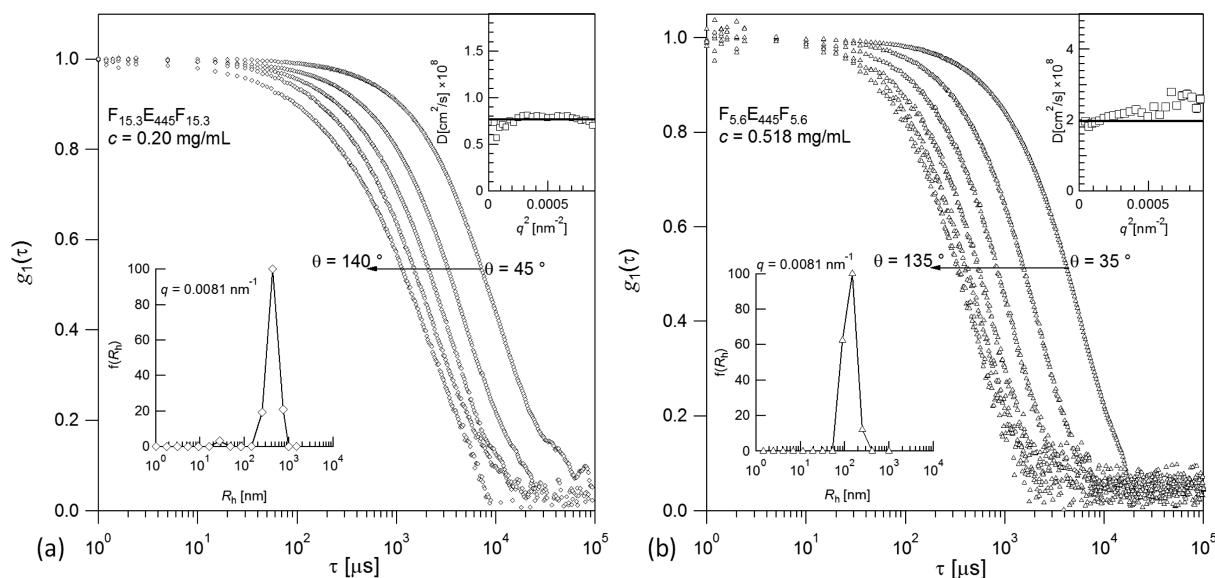


Figure 6. Typical normalized DLS correlation function, showing every 20° for clarity, fit by quadratic cumulant method for $F_{15.3}E_{445}F_{15.3}$ (a) and $F_{5.6}E_{445}F_{5.6}$ (b). The inset at right top is $D = \bar{\Gamma}/q^2$ versus q^2 plot, while inset at left bottom shows CONTIN confirming one mode.

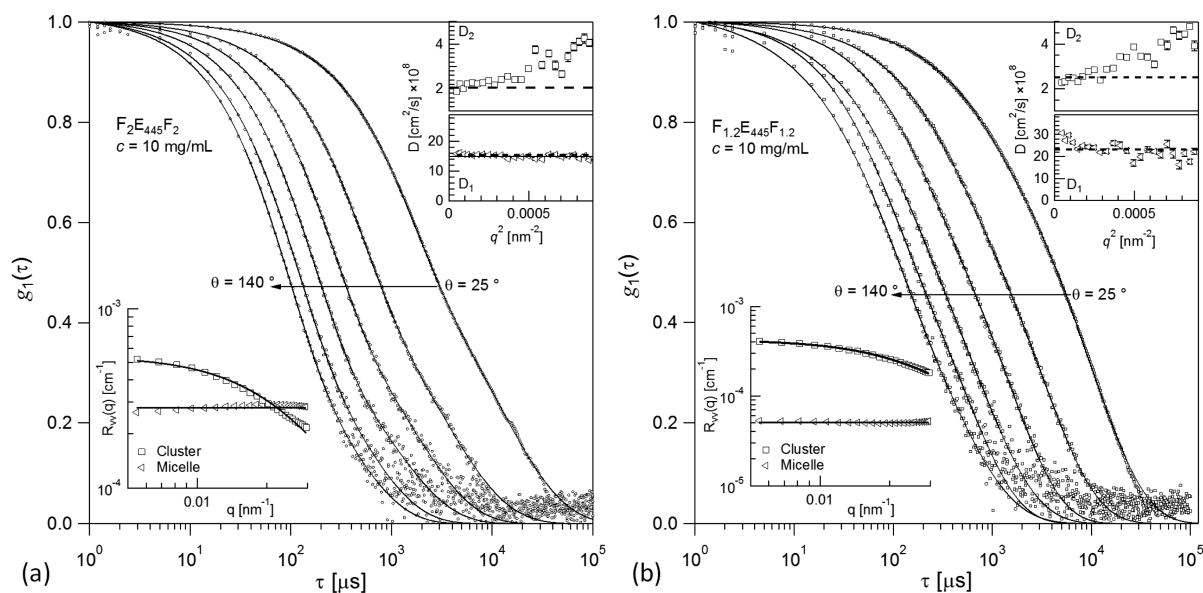


Figure 7. Typical normalized DLS correlation function, shown for every 20° for clarity, with fits by eq 3 for $F_2E_{445}F_2$ (a) and $F_{1.2}E_{445}F_{1.2}$ (b). Lower left inset are the DLS amplitude-weighted light scattering from micelle ($I_1(q)$, \triangleleft) and cluster ($I_2(q)$, \square). Upper right inset are the effective diffusion coefficient for each mode.

not within the resolution of light scattering, but neutron scattering.²⁹

Figure 8 shows the concentration dependence of the hydrodynamic radius estimated by the plateau values of D for $F_{15.3}E_{445}F_{15.3}$ and $F_{5.6}E_{445}F_{5.6}$. The R_h values show a larger polydispersity near the CMC with error bars representing the polydispersity from the cumulant analysis. These results suggest that the average size is due to the formation of clusters without clear separation into single micelles by DLS. The mean R_h values of $F_{15.3}E_{445}F_{15.3}$ in $20 < c/\text{CMC} < 200 \approx 255 \pm 10$ nm and $F_{5.6}E_{445}F_{5.6} \approx 100 \pm 1$ nm show a nearly concentration-independent scaling of the cluster size with c/CMC that do not dissociate substantially upon dilution.

$F_2E_{445}F_2$ and $F_{1.2}E_{445}F_{1.2}$ were studied by small-angle neutron scattering and modeled as star-like micelles with hydrophobic

oligocarbonate fluorene point-like core and hydrophilic PEG outer shell that form chain-like clusters.²⁹ As shown in Figure 9, R_h determined from micelles (D_1) remains constant, whereas the R_h from the clusters (D_2) increases with concentration. For $F_2E_{445}F_2$, micelle $R_h \approx 16.4 \pm 0.1$ nm and cluster R_h increases from 38 to 101 nm as concentration increases from 2.0 to 10 mg/mL. For $F_{1.2}E_{445}F_{1.2}$, micelle $R_h \approx 11.8 \pm 0.8$ nm and cluster size R_h increases from 36 to 92 nm within the concentration range 1.25–10 mg/mL. The concentration dependence of the cluster R_h shows an equilibrium between micelles and clusters within the strong clustering regime defined by Figure 4. As concentration increases, the equilibrium shifts toward the clusters as confirmed by the reduced scattered intensities in Figure 4 and the DLS amplitudes (Figure S4). This behavior is a signature of self-assembly.^{64,65}

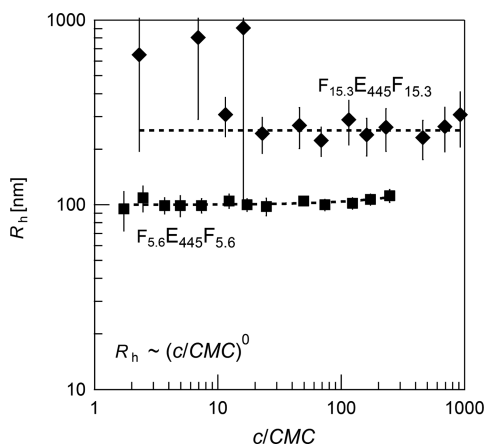


Figure 8. Cluster hydrodynamic radius for $F_{15.3}E_{445}F_{15.3}$ and $F_{5.6}E_{445}F_{5.6}$. The error bars represent one standard deviation of the size polydispersity obtained from the cumulant analysis.

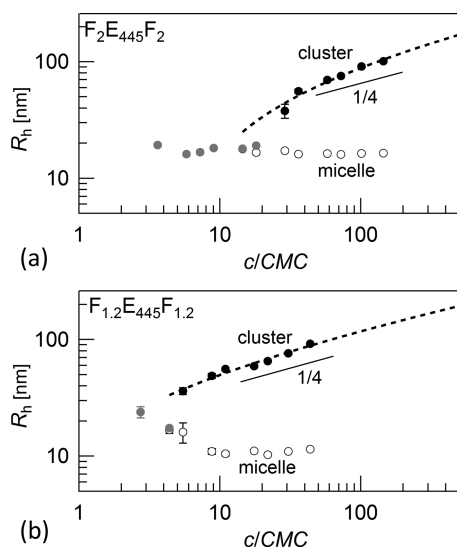


Figure 9. Concentration dependence of hydrodynamic radius (R_h) of the micelle and cluster for (a) $F_2E_{445}F_2$ and (b) $F_{1.2}E_{445}F_{1.2}$. Black circles represent the data fit by single exponential function. Black spheres represent the data fit by stretched exponential function. Gray spheres represent the data fit by cumulant method when single modes are observed. Dotted line is mean field open assembly model described in the text.

Strong Clustering Regime: Closed Assembly Coupled to Open Assembly. The observation of micellization and micelle clustering implies a hierarchical assembly enabled by F-TMC. The self-assembly of small-molecule or polymer amphiphiles into micelles is a closed assembly process.⁶⁶ In this case a narrow distribution of associated species is present in significant proportion. A single equilibrium may approximate the concentration of unimers (M_1) and associated species ($M_{\tilde{N}}$) of finite size, such that $\tilde{N}M_1 = M_{\tilde{N}}$, where \tilde{N} is the association number.^{51,66} This closed assembly model⁶⁷ assumes a CMC, below which only unimers are present and above which micelles can be detected with equilibrium constant $K_{\tilde{N}}^c = [M_{\tilde{N}}]/[M_1]^{\tilde{N}}$.

If further association of micelles occurs, then a hierarchical assembly model is necessary. As an approximation, we assume that the micelles remain intact and follow a multistep equilibrium.^{66,67} The formation of an \tilde{L} -mer of micelles occurs

via a stepwise association with equilibrium constant $K_{\tilde{L}}$ given by $K_{\tilde{L}} = [M_{(\tilde{N})\tilde{L}}]/[M_{(\tilde{N})\tilde{L}-1}][M_{\tilde{N}}]$. If for each step K_i is approximately equal, the associated species would have a broad size distribution. This case is referred to as open assembly in the polymer^{51,66} and small molecule surfactant^{67,68} literature. Mukerjee⁶⁷ showed that with this model the average degree of association, \tilde{L} , proportional to mass-average molecular mass, scales as $\tilde{L} = 2\sqrt{K/K_2}\sqrt{c/CMC}$. This prediction depends upon the ratio of two equilibrium constants one to form a dimer (K_2) and equal equilibria (K) for all other higher-order stepwise associations. This prediction may be compared to the experimental data in Figures 5 and 9 by invoking Gaussian statistics for the cluster size, $R^2 \sim \tilde{L}l^2$ with step length l leading to $R \sim (c/CMC)^{1/4}$.

Figure 9 shows the general agreement with the equilibrium open assembly model shown as the dotted line and compared to the scaling in Figure 5. Therefore, the equilibrium assembly of $F_2E_{445}F_2$ and $F_{1.2}E_{445}F_{1.2}$ is a closed, coupled to open assembly process. In the strong clustering regime, as the polymer concentration increases, more micelles form, and these micelles reversibly associate into clusters mediated by F-TMC groups via bridging interaction.

In the absence of a hierarchical multiequilibria model, the worm-like micelle theory of Cates and Candau⁶⁹ predicts the mean contour length, \tilde{L} , follows the concentration scaling $\tilde{L} \sim c^{1/2} \exp(E/2k_B T)$, where E is a scission energy.^{69,70} Within Gaussian statistics, $R_g \sim c^{1/4}$, which is identical to the multiequilibria model. Branching may be included in either estimate as discussed by Burchard.⁷¹

Observations of Intracluster Relaxations. Internal relaxations could be observed if the structures are sufficiently flexible in the $qR_g > 1$ limit.⁷² The systematic DLS study over a wide concentration and q -range of $F_mE_{445}F_m$ reveals internal dynamics of clusters. The analysis for $F_{5.6}E_{445}F_{5.6}$, $F_2E_{445}F_2$, and $F_{1.2}E_{445}F_{1.2}$ observes a deviation in the effective diffusion coefficient from Figures 6b, 7a, and 7b. This deviation is attributed to the crossover of the decay rate dependence from q^2 to q^3 . Further, the model fit stretched exponent β is independent of q (Figures S5 and S6). The normal mode relaxations from Gaussian polymer chains with hydrodynamic interactions follow Rouse–Zimm dynamics with a q^3 -dependent relaxation rate (Γ_2) and stretched exponent $\beta = 2/3$ as a limiting law.⁷³ Relaxations that occur within the clusters are consistent with Rouse–Zimm dynamics for the data shown in Figure 10.

Figure 10 shows the dimensionless plot of $(\Gamma_2/q^3)/(k_B T/\eta_0)$ as a function of $(q(R_g))^2$ for $F_2E_{445}F_2$ and $F_{1.2}E_{445}F_{1.2}$ at $c > CMC$. The dimensionless plot for the normalized decay rate by the correct Rouse–Zimm variables eliminates the solvent viscosity and temperature dependence. Further, the normalized $q(R_g)$ axis shows the probe scale less than or greater than the $\langle R_g \rangle$ of the cluster. The values of $(\Gamma_2/q^3)/(k_B T/\eta_0)$ plateau near $(q(R_g))^2 > 1.5$. This plateau for linear polymer solutions is typically between 0.05 and 0.06^{74–76} and frequently lower than the theoretical prediction of 0.071 and 0.079 with and without a preaveraged Oseen tensor, respectively.⁷⁷

We consider two possibilities to this lower plateau. A lower plateau was explained by Wu et al. as related to a key assumption in the dynamics theory that energetically favorable internal motions are not observable in DLS at a particular $q(R_g)$ due to finite cutoff observation length scale $1/q$.⁷⁵ Therefore, if internal motions do not contribute to the measured spectrum,

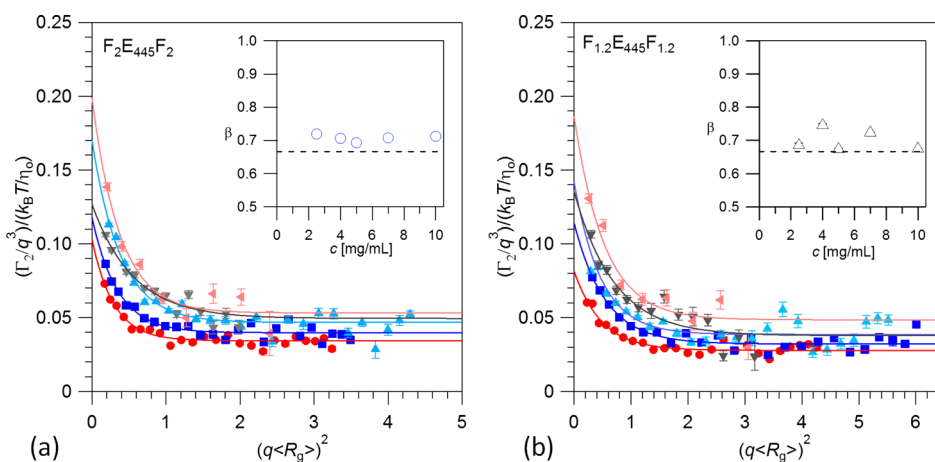


Figure 10. Variation of $(\Gamma_2/q^3)/(k_B T/\eta_0)$ as a function of $(q\langle R_g \rangle)^2$ for (a) $F_2E_{445}F_2$ and (b) $F_{1.2}E_{445}F_{1.2}$ at different concentrations (●, 10 mg/mL; ■, 7 mg/mL; ▲, 5 mg/mL; ▼, 4 mg/mL; and ◀, 2.5 mg/mL) with solid lines are guides to the eye. Inset shows the concentration dependence of the average stretched exponent β with dotted line showing the Rouse–Zimm limiting value ($\beta = 2/3$).

the calculated Γ should be smaller than the predicted Rouse–Zimm model. This smaller Γ will lead to a lower plateau value. The consideration of the dynamics using a stretched exponential integrates over all normal modes is an approximate model.⁷³ In Figure 10, the observed plateau values of $(\Gamma_2/q^3)/(k_B T/\eta_0)$ are in the range of 0.035–0.055. Wu et al. observed similar behavior for well-defined PNIPAM covalently cross-linked microgel particles when compared to linear chains.⁷⁶ The plateau value of PNIPAM microgel particles is ≈ 3.5 times lower than that of linear PNIPAM (≈ 0.05), since the internal motions of the microgel are suppressed by covalent cross-linking. In the present case, interconnected micelles within a cluster serves as effective beads connected by entropic bridging chains. This view complements the observations with microgels synthesized through covalent cross-linking. Observations by Wu et al.⁷⁶ with well-defined microgels additionally show that a linear association is not necessary to observe Zimm-like dynamics.

Another consideration for the concentration dependence of the plateau is that the local solvent viscosity is not that of the bulk. The plateau of $(\Gamma_2/q^3)/(k_B T/\eta_0)$ shows a systematic concentration dependence. A plot of the $q^3 k_B T/\Gamma_2$ plateau versus c provides an apparent local solvent viscosity (Figure S7). However, the magnitude of the local viscosity increase does not seem reasonable to be the only source of the fractional increase in the apparent local solvent viscosity, when considering the literature data for polymers in organic and halogenated solvents.^{78,79} Gisser et al. showed that the relative diffusivity of tetrahydrofuran solvent does slow down in the presence of polystyrene.⁸⁰ However, in order to observe an $\approx 10\%$ slowing down in solvent diffusivity the volume fraction of polymer would need to be ≈ 0.07 . A conservative estimate for the volume fraction of polymers within the clusters, using the Zimm plot results, is between 0.02 and 0.05. This subtle effect requires molecular dynamics simulations to understand the local hydrodynamic coupling between solvent and polymer or, in this case, micelle within cluster and solvent. Recent studies on PEO by Mondal et al. would provide insight when focused on the water dynamics in the vicinity of the polymer.⁸¹

Microgel-like Clusters Become More Isotropic at Higher Concentration. The ratio $\rho = \langle R_g \rangle / \langle R_h \rangle$ quantifies shape anisotropy.⁸² Estimates for ρ were updated using modern numerical methods to calculate the frictional and hydrodynamic

properties of objects formed by a variety of association mechanisms as reviewed by Mansfield and Douglas.⁸³ These theoretical considerations conclude that equilibrium self-similar clusters tend to be anisotropic, whereas nonequilibrium clusters

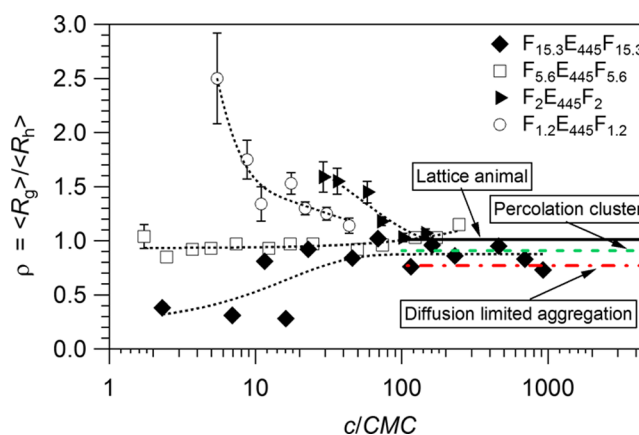


Figure 11. CMC-normalized concentration dependence of the ratio of the cluster apparent radius of gyration (R_g) to the clusters hydrodynamic radius (R_h). The dotted lines are guides to the eye. The asymptotic values for lattice animals, percolation clusters, and diffusion limited aggregation are provided by the solid, dashed, and dash-dotted lines, respectively.

are more isotropic. Figure 11 summarizes ρ as a function of c/CMC within the strong clustering regime. $F_{1.2}E_{445}F_{1.2}$ and $F_2E_{445}F_2$ at lower c/CMC have initially higher ρ values that decrease to near unity. $F_{5.6}E_{445}F_{5.6}$ is near unity across the entire concentration range, and $F_{15.3}E_{445}F_{15.3}$ has global values of ρ that increases with concentration. A universal feature is a tendency toward a similar ρ with increasing c/CMC .

Just above the CMC, highly anisotropic clusters are observed for lower m that transitions to more compact clusters as m increases from 1.2 to 15.3. This appears to correlate with the clusters that display internal relaxation modes ($m = 1.2, 2,$ and 5.6) and those which are not apparent ($m = 15.3$). Perhaps the most compact clusters do not exhibit the internal relaxation modes visible to DLS length scales due to the high extent of micelle interconnectivity as concluded by the microgel studies

of Wu and Zhou.⁷⁶ Measurements that unambiguously quantify the interconnectivity are needed.

The observed shape anisotropy of the clusters connects to theoretical predictions (Figure 11). Self-similar equilibrium clusters predict anisotropic shapes with larger ρ . This is observed for lower c/CMC of $F_{1.2}E_{445}F_{1.2}$ and $F_2E_{445}F_2$. It is not unreasonable to deduce that at lower concentrations the clusters appear more anisotropic, then as the extent of clustering increases, the clusters plateau at a lower value of ρ , implying less anisotropy, still far from the isotropic uniform sphere value of 0.775 expected for nonequilibrium clusters. $F_{5.6}E_{445}F_{5.6}$ exhibits very little dependence with c/CMC with a plateau value of $\rho \approx 1$. $F_{15.3}E_{445}F_{15.3}$ has a larger variability but lower values in ρ at low concentration that rises to between 0.78 and 1.0. $F_{15.3}E_{445}F_{15.3}$ has the most compact and isotropic structures better described by nonequilibrium clusters (e.g., diffusion-limited aggregation), whereas $F_{5.6}E_{445}F_{5.6}$, $F_2E_{445}F_2$, and $F_{1.2}E_{445}F_{1.2}$ are self-similar and equilibrium clusters (e.g., percolation clusters and lattice animals).

Upon increasing the symmetric end-group degree of polymerization the window of micelle and clusters formation grows. However, within the m - c state diagram of Figure 3, the clustering assembly mechanisms are different. The formation of clusters having similar shape anisotropy with increasing c/CMC was a universal feature. By comparing the cluster size and anisotropy ratio to mean-field models, one can begin to quantify the nonequilibrium and equilibrium cluster structures. In our system, we note that telechelic polymers with highly hydrophobic ends may have limited water solubility, which may be more common than often discussed in block copolymer micelles and gels for drug encapsulation and delivery. A common route to form micelles is to predissolve in a common organic solvent and dialyze⁸⁴ to obtain desired structures as was done with $F_{15.3}E_{445}F_{15.3}$ and $F_{5.6}E_{445}F_{5.6}$. $F_{5.6}E_{445}F_{5.6}$ exhibited a slight increase in the $\langle R_g \rangle$ of the cluster with increasing concentration, while $F_{15.3}E_{445}F_{15.3}$ did not. This is most likely the persistence of flower-like micelles,^{85,86} whereby the enthalpic penalty to permit free ends and kinetics of assembly are prohibitively slow making self-assembly kinetically controlled. However, $F_2E_{445}F_2$ and $F_{1.2}E_{445}F_{1.2}$ are immediately soluble and reversibly assembled, a desirable feature for drug encapsulating particles and injectable gels. Figure 3 needs to consider the interaction parameters. For instance, the strong self-association of the fluorene groups suggests a large Flory–Huggins interaction parameter. This not only drives the selected solubility and micellization but also kinetically prevents dissolution and formation of well-defined structures. Figure 3 may be better considered and made universal by the product $\chi_{AS}m$. This work is ongoing with selective deuterium labeling and small-angle neutron scattering.

CONCLUSION

The supramolecular assembly of $F_mE_{445}F_m$ telechelic (triblock) polymers exhibits a classical critical micelle concentration. This closed-assembly process becomes coupled to micelle clustering with increasing concentration and end-group degree of polymerization, m . The concentration dependence for the cluster size was consistent with mean-field descriptions derived for worm-like chain assembly and multistep equilibrium models. Without any adjustment, experimental data follow the mean-field scaling $R \sim (c/\text{CMC})^{1/4}$. At low m , clusters are anisotropic near the CMC and become more isotropic with increasing concentration as quantified by the anisotropy ratio.

Moreover, low m clusters resemble soft microgels through their internal dynamics when compared to well-defined cross-linked microgels. The internal dynamics of these clusters are consistent with Rouse–Zimm dynamics. This behavior is strongly dependent on m . Higher m values do not show the q^3 deviations in the q^2 decay rate law expected by translational diffusion. These tend to be irreversible isotropic clusters through their anisotropy ratio. These observations demonstrate that incorporation of F-TMC groups leads to classical micelles that are coupled to hierarchical assembly (clustering of micelles). This closed, coupled-to open assembly is a general process readily probed by angular-dependent static and dynamic light scattering. Since solution and gel properties (viscosity, shear modulus) and delivery properties (encapsulation, release, loading) are always dependent upon the microstructure, these experiments provide a detailed view on the fundamentals of supramolecular driven assembly.

ASSOCIATED CONTENT

Supporting Information

The Supporting Information is available free of charge on the ACS Publications website at DOI: 10.1021/acs.macromol.6b02524.

Parameters from static light scattering by eq 4, Berry plot from $R_w(c,q)$, Zimm plot from $I_2(c,q)$, angular dependence of the scattered light intensity $I_2(q)$ and $[R_w(q)]^{1/2}$, concentration dependence of the relative amplitude of micelle (a_1) and cluster (a_2), q dependence of the stretched exponent β , local solvent viscosity, and examples of CONTIN results (PDF)

AUTHOR INFORMATION

Corresponding Author

*E-mail vprabhu@nist.gov, Tel (301) 975-3657 (V.M.P.).

ORCID

Yi Yan Yang: 0000-0002-1871-5448

James L. Hedrick: 0000-0002-3621-9747

Vivek M. Prabhu: 0000-0001-8790-9521

Notes

The authors declare no competing financial interest.

ACKNOWLEDGMENTS

Y.Y.Y. and S.V. acknowledge funding support from the Institute of Bioengineering and Nanotechnology (Biomedical Research Council, Agency for Science, Technology and Research, Singapore). V.M.P. and G.W. thank Jack Douglas (NIST) for stimulating discussions and the support of the NIST Materials Genome Initiative, R. L. Jones, Director of the *n*SOFT beamline at the NIST Center for Neutron Research, and W. Vreeland (NIST) for assistance in the refractive index increment measurements.

ADDITIONAL NOTE

^ACertain commercial equipment and materials are identified in this paper in order to specify adequately the experimental procedure. In no case does such identification imply recommendations by the National Institute of Standards and Technology (NIST) nor does it imply that the material or equipment identified is necessarily the best available for this purpose.

REFERENCES

- (1) Nakanishi, T.; Fukushima, S.; Okamoto, K.; Suzuki, M.; Matsumura, Y.; Yokoyama, M.; Okano, T.; Sakurai, Y.; Kataoka, K. Development of the Polymer Micelle Carrier System for Doxorubicin. *J. Controlled Release* **2001**, *74* (1–3), 295–302.
- (2) Huh, K. M.; Min, H. S.; Lee, S. C.; Lee, H. J.; Kim, S.; Park, K. A New Hydrotropic Block Copolymer Micelle System for Aqueous Solubilization of Paclitaxel. *J. Controlled Release* **2008**, *126* (2), 122–129.
- (3) Cabral, H.; Kataoka, K. Progress of Drug-Loaded Polymeric Micelles into Clinical Studies. *J. Controlled Release* **2014**, *190*, 465–476.
- (4) Wibowo, A.; Osada, K.; Matsuda, H.; Anraku, Y.; Hirose, H.; Kishimura, A.; Kataoka, K. Morphology Control in Water of Polyion Complex Nanoarchitectures of Double-Hydrophilic Charged Block Copolymers through Composition Tuning and Thermal Treatment. *Macromolecules* **2014**, *47* (9), 3086–3092.
- (5) Feldman, K. E.; Kade, M. J.; de Greef, T. F. A.; Meijer, E. W.; Kramer, E. J.; Hawker, C. J. Polymers with Multiple Hydrogen-Bonded End Groups and Their Blends. *Macromolecules* **2008**, *41* (13), 4694–4700.
- (6) Fukushima, K.; Tan, J. P. K.; Korevaar, P. A.; Yang, Y. Y.; Pitera, J.; Nelson, A.; Maune, H.; Coody, D. J.; Frommer, J. E.; Engler, A. C.; Huang, Y.; Xu, K.; Ji, Z.; Qiao, Y.; Fan, W.; Li, L.; Wiradharma, N.; Meijer, E. W.; Hedrick, J. L. Broad-Spectrum Antimicrobial Supramolecular Assemblies with Distinctive Size and Shape. *ACS Nano* **2012**, *6* (10), 9191–9199.
- (7) Kutz, A.; Mariani, G.; Groehn, F. Ionic Dye-Surfactant Nanoassemblies: Interplay of Electrostatics, Hydrophobic Effect, and Pi-Pi Stacking. *Colloid Polym. Sci.* **2016**, *294* (3), 591–606.
- (8) Marakis, J.; Wunderlich, K.; Klapper, M.; Vlassopoulos, D.; Fytas, G.; Müllen, K. Strong Physical Hydrogels from Fibrillar Supramolecular Assemblies of Poly(ethylene Glycol) Functionalized Hexaphenylbenzenes. *Macromolecules* **2016**, *49* (9), 3516–3525.
- (9) Lin, S.; Lin, J.; Nose, T.; Iyoda, T. Micellar Structures of Block-Copolymers with Ordered Cores in Dilute Solution as Studied by Polarized and Depolarized Light Scattering. *J. Polym. Sci., Part B: Polym. Phys.* **2007**, *45* (11), 1333–1343.
- (10) Jia, L.; Levy, D.; Durand, D.; Imperor-Clerc, M.; Cao, A.; Li, M.-H. Smectic Polymer Micellar Aggregates with Temperature-Controlled Morphologies. *Soft Matter* **2011**, *7* (16), 7395–7403.
- (11) Agrawal, S. K.; Sanabria-DeLong, N.; Tew, G. N.; Bhatia, S. R. Structural Characterization of PLA-PEO-PLA Solutions and Hydrogels: Crystalline vs Amorphous PLA Domains. *Macromolecules* **2008**, *41* (5), 1774–1784.
- (12) Zinn, T.; Willner, L.; Pipich, V.; Richter, D.; Lund, R. Effect of Core Crystallization and Conformational Entropy on the Molecular Exchange Kinetics of Polymeric Micelles. *ACS Macro Lett.* **2015**, *4* (6), 651–655.
- (13) Agrawal, S. K.; Sanabria-DeLong, N.; Tew, G. N.; Bhatia, S. R. Rheological Characterization of Biocompatible Associative Polymer Hydrogels with Crystalline and Amorphous Endblocks. *J. Mater. Res.* **2006**, *21* (8), 2118–2125.
- (14) Lee, A. L. Z.; Venkataraman, S.; Fox, C. H.; Coody, D. J.; Frank, C. W.; Hedrick, J. L.; Yang, Y. Y. Modular Composite Hydrogels from Cholesterol-Functionalized Polycarbonates for Antimicrobial Applications. *J. Mater. Chem. B* **2015**, *3* (34), 6953–6963.
- (15) Lee, A. L. Z.; Ng, V. W. L.; Gao, S.; Hedrick, J. L.; Yang, Y. Y. Injectable Biodegradable Hydrogels from Vitamin D-Functionalized Polycarbonates for the Delivery of Avastin with Enhanced Therapeutic Efficiency against Metastatic Colorectal Cancer. *Biomacromolecules* **2015**, *16* (2), 465–475.
- (16) Lee, A. L. Z.; Ng, V. W. L.; Wang, W.; Hedrick, J. L.; Yang, Y. Y. Block Copolymer Mixtures as Antimicrobial Hydrogels for Biofilm Eradication. *Biomaterials* **2013**, *34* (38), 10278–10286.
- (17) Yang, Z.; Pickard, S.; Deng, N.-J.; Barlow, R. J.; Attwood, D.; Booth, C. Effect of Block Structure on the Micellization and Gelation of Aqueous Solutions of Copolymers of Ethylene Oxide and Butylene Oxide. *Macromolecules* **1994**, *27* (9), 2371–2379.
- (18) Yang, Y.-W.; Yang, Z.; Zhou, Z.-K.; Attwood, D.; Booth, C. Association of Triblock Copolymers of Ethylene Oxide and Butylene Oxide in Aqueous Solution. A Study of B N E M B N Copolymers. *Macromolecules* **1996**, *29* (2), 670–680.
- (19) Liu, T.; Zhou, Z.; Wu, C.; Chu, B.; Schneider, D. K.; Nace, V. M. Self-Assembly of Poly (Oxybutylene)-Poly (Oxyethylene)-Poly (oxybutylene)(B6E46B6) Triblock Copolymer in Aqueous Solution. *J. Phys. Chem. B* **1997**, *101* (43), 8808–8815.
- (20) Liu, T. B.; Zhou, Z. K.; Wu, C. H.; Nace, V. M.; Chu, B. Dominant Factors on the Micellization of BnEmBn-Type Triblock Copolymers in Aqueous Solution. *J. Phys. Chem. B* **1998**, *102* (16), 2875–2882.
- (21) Zhou, Z. K.; Chu, B.; Nace, V. M.; Yang, Y. W.; Booth, C. Self-Assembly Characteristics of BEB-Type Triblock Copolymers. *Macromolecules* **1996**, *29* (10), 3663–3664.
- (22) Zhou, Z.; Chu, B.; Nace, V. M. Association Behavior of a Triblock Copolymer of Oxyethylene (E) and Oxybutylene (B). A Study of BSE91B5 in Aqueous Solution. *Langmuir* **1996**, *12* (21), 5016–5021.
- (23) Zhou, Z.; Chu, B. Phase-Behavior and Association Properties of Poly(oxypropylene)-Poly(oxyethylene)-Poly(oxypropylene) Triblock Copolymer in Aqueous-Solution. *Macromolecules* **1994**, *27* (8), 2025–2033.
- (24) Kumi, B. C.; Hammouda, B.; Greer, S. C. Self-Assembly of the Triblock Copolymer 17R4 Poly(propylene oxide)(14)-Poly(ethylene oxide)(24)-Poly(propylene oxide)(14) in D₂O. *J. Colloid Interface Sci.* **2014**, *434*, 201–207.
- (25) Ci, T.; Li, T.; Chen, L.; Chang, G.; Yu, L.; Ding, J. Effects Of “mature Micelle” formation of Pluronic P123 on Equilibrium between Lactone and Carboxylate Forms of 10-Hydrocamptothecin in Water. *Polym. Chem.* **2013**, *4* (11), 3245–3255.
- (26) Ho, D. L.; Hammouda, B.; Kline, S. R. Clustering of Poly(ethylene Oxide) in Water Revisited. *J. Polym. Sci., Part B: Polym. Phys.* **2003**, *41* (1), 135–138.
- (27) Hammouda, B.; Ho, D. L.; Kline, S. Insight into Clustering in Poly(ethylene Oxide) Solutions. *Macromolecules* **2004**, *37* (18), 6932–6937.
- (28) Hammouda, B. The Mystery of Clustering in Macromolecular Media. *Polymer* **2009**, *50* (22), 5293–5297.
- (29) Prabhu, V. M.; Venkataraman, S.; Yang, Y. Y.; Hedrick, J. L. Star-Like Structure of Oligocarbonate-Fluorene End-Functionalized Poly(ethylene Glycol) ABA Triblock Copolymers Below the Gel Point. *Macromol. Symp.* **2015**, *358* (1), 157–169.
- (30) Higgins, J. S.; Benoit, H. C. *Polymers and Neutron Scattering*; Oxford University Press: New York, 1994.
- (31) Prabhu, V. M.; Venkataraman, S.; Yang, Y. Y.; Hedrick, J. L. Equilibrium Self-Assembly, Structure, and Dynamics of Clusters of Star-Like Micelles. *ACS Macro Lett.* **2015**, *4* (10), 1128–1133.
- (32) Vagberg, L. J.; Cogan, K. A.; Gast, A. P. Light-Scattering Study of Starlike Polymeric Micelles. *Macromolecules* **1991**, *24* (7), 1670–1677.
- (33) Wu, H. Correlations between the Rayleigh Ratio and the Wavelength for Toluene and Benzene. *Chem. Phys.* **2010**, *367* (1), 44–47.
- (34) Debye, P. Molecular-Weight Determination by Light Scattering. *J. Phys. Colloid Chem.* **1947**, *51* (1), 18–32.
- (35) Zimm, B. H. The Scattering of Light and the Radial Distribution Function of High Polymer Solutions. *J. Chem. Phys.* **1948**, *16* (12), 1093–1099.
- (36) Berry, G. C. Thermodynamic and Conformational Properties of Polystyrene. I. Light-Scattering Studies on Dilute Solutions of Linear Polystyrenes. *J. Chem. Phys.* **1966**, *44* (12), 4550–4564.
- (37) Adams, D. J.; Adams, S.; Atkins, D.; Butler, M. F.; Fuzeland, S. Impact of Mechanism of Formation on Encapsulation in Block Copolymer Vesicles. *J. Controlled Release* **2008**, *128* (2), 165–170.
- (38) Fytas, G. Light Scattering from Dense Polymer Systems. In *Scattering: Scattering and Inverse Scattering in Pure and Applied Science*; Academic Press: San Diego, CA, 2003; Vol. 35, pp 849–863.

- (39) Provencher, S. W. CONTIN: A General Purpose Constrained Regularization Program for Inverting Noisy Linear Algebraic and Integral Equations. *Comput. Phys. Commun.* **1982**, *27* (3), 229–242.
- (40) Frisken, B. J. Revisiting the Method of Cumulants for the Analysis of Dynamic Light-Scattering Data. *Appl. Opt.* **2001**, *40* (24), 4087–4091.
- (41) Venkataraman, S.; L. Hedrick, J.; Yan Yang, Y. Fluorene-Functionalized Aliphatic Polycarbonates: Design, Synthesis and Aqueous Self-Assembly of Amphiphilic Block Copolymers. *Polym. Chem.* **2014**, *5* (6), 2035–2040.
- (42) Nakano, T.; Takewaki, K.; Yade, T.; Okamoto, Y. Dibenzofulvene, a 1, 1-Diphenylethylene Analogue, Gives a π -Stacked Polymer by Anionic, Free-Radical, and Cationic Catalysts. *J. Am. Chem. Soc.* **2001**, *123* (37), 9182–9183.
- (43) Nakano, T. Synthesis, Structure and Function of π -Stacked Polymers. *Polym. J.* **2010**, *42* (2), 103–123.
- (44) Liu, C.-L.; Lin, C.-H.; Kuo, C.-C.; Lin, S.-T.; Chen, W.-C. Conjugated Rod-coil Block Copolymers: Synthesis, Morphology, Photophysical Properties, and Stimuli-Responsive Applications. *Prog. Polym. Sci.* **2011**, *36* (5), 603–637.
- (45) Tuzar, Z.; Koňák, Č.; Štěpánek, P.; Pleštil, J.; Kratochvíl, P.; Prochazka, K. Dilute and Semidilute Solutions of ABA Block Copolymer in Solvents Selective for A or B Blocks. 2. Light Scattering and Sedimentation Study. *Polymer* **1990**, *31* (11), 2118–2124.
- (46) Quintana, J. R.; Villacampa, M.; Katime, I. A. Micellization of a Polystyrene-B-Poly (Ethylene/Propylene) Block Copolymer in N-Dodecane/1, 4-Dioxane Mixtures. 2. Structure and Dimensions of Micelles. *Macromolecules* **1993**, *26* (4), 606–611.
- (47) Khougaz, K.; Gao, Z.; Eisenberg, A. Determination of the Critical Micelle Concentration of Block Copolymer Micelles by Static Light Scattering. *Macromolecules* **1994**, *27* (22), 6341–6346.
- (48) Nolan, S. L.; Phillips, R. J.; Cotts, P. M.; Dungan, S. R. Light Scattering Study on the Effect of Polymer Composition on the Structural Properties of PEO–PPO–PEO Micelles. *J. Colloid Interface Sci.* **1997**, *191* (2), 291–302.
- (49) Harada, A.; Kataoka, K. Novel Polyion Complex Micelles Entrapping Enzyme Molecules in the Core. 2. Characterization of the Micelles Prepared at Nonstoichiometric Mixing Ratios. *Langmuir* **1999**, *15* (12), 4208–4212.
- (50) Gao, Z.; Eisenberg, A. A Model of Micellization for Block Copolymers in Solutions. *Macromolecules* **1993**, *26* (26), 7353–7360.
- (51) Price, C. Micelle Formation by Block Copolymers in Organic Solvents. *Pure Appl. Chem.* **1983**, *55* (10), 1563–1572.
- (52) Huibers, P. D.; Lobanov, V. S.; Katritzky, A. R.; Shah, D. O.; Karelson, M. Prediction of Critical Micelle Concentration Using a Quantitative Structure-Property Relationship Approach. 1. Nonionic Surfactants. *Langmuir* **1996**, *12* (6), 1462–1470.
- (53) Astafieva, I.; Zhong, X. F.; Eisenberg, A. Critical Micellization Phenomena in Block Polyelectrolyte Solutions. *Macromolecules* **1993**, *26* (26), 7339–7352.
- (54) Lodge, T. P.; Muthukumar, M. Physical Chemistry of Polymers: Entropy, Interactions, and Dynamics. *J. Phys. Chem.* **1996**, *100* (31), 13275–13292.
- (55) Marko, J. F.; Rabin, Y. Microphase Separation of Charged Diblock Copolymers: Melts and Solutions. *Macromolecules* **1992**, *25* (5), 1503–1509.
- (56) Devanand, K.; Selser, J. C. Asymptotic Behavior and Long-Range Interactions in Aqueous Solutions of Poly (Ethylene Oxide). *Macromolecules* **1991**, *24* (22), 5943–5947.
- (57) Tanaka, F. Theory of Thermoreversible Gelation. *Macromolecules* **1989**, *22* (4), 1988–1994.
- (58) Dutertre, F.; Bang, K.-T.; Loppinet, B.; Choi, I.; Choi, T.-L.; Fytas, G. Structure and Dynamics of Dendronized Polymer Solutions: Gaussian Coil or Macromolecular Rod? *Macromolecules* **2016**, *49* (7), 2731–2740.
- (59) Beer, M.; Schmidt, M.; Muthukumar, M. The Electrostatic Expansion of Linear Polyelectrolytes: Effects of Gegenions, Co-Ions, and Hydrophobicity. *Macromolecules* **1997**, *30* (26), 8375–8385.
- (60) Nguyen-Misra, M.; Mattice, W. L. Micellization and Gelation of Symmetric Triblock Copolymers with Insoluble End Blocks. *Macromolecules* **1995**, *28* (5), 1444–1457.
- (61) Khalatur, P. G.; Khokhlov, A. R.; Kovalenko, J. N.; Mologin, D. A. Molecular Dynamics Study of the Solution of Semiflexible Telechelic Polymer Chains with Strongly Associating End-Groups. *J. Chem. Phys.* **1999**, *110* (12), 6039–6049.
- (62) von Berlepsch, H.; Harnau, L.; Reineker, P. Persistence Length of Wormlike Micelles from Dynamic Light Scattering. *J. Phys. Chem. B* **1998**, *102* (39), 7518–7522.
- (63) Martin, J. E.; Wilcoxon, J.; Odinek, J. Decay of Density Fluctuations in Gels. *Phys. Rev. A: At, Mol., Opt. Phys.* **1991**, *43* (2), 858.
- (64) Raspaud, E.; Lairez, D.; Adam, M.; Carton, J.-P. Triblock Copolymers in a Selective Solvent. I. Aggregation Process in Dilute Solution. *Macromolecules* **1994**, *27* (11), 2956–2964.
- (65) Douglas, J. F.; Dudowicz, J.; Freed, K. F. Lattice Model of Equilibrium Polymerization. VII. Understanding the Role of “cooperativity” in Self-Assembly. *J. Chem. Phys.* **2008**, *128* (22), 224901.
- (66) Elias, H.-G. *Light Scattering from Polymer Solutions*; Academic Press: New York, 1972; p 397.
- (67) Mukerjee, P. Size Distribution of Small and Large Micelles. Multiple Equilibrium Analysis. *J. Phys. Chem.* **1972**, *76* (4), 565–570.
- (68) Martin, R. B. Comparisons of Indefinite Self-Association Models. *Chem. Rev.* **1996**, *96* (8), 3043–3064.
- (69) Cates, M. E.; Candau, S. J. Statics and Dynamics of Worm-like Surfactant Micelles. *J. Phys.: Condens. Matter* **1990**, *2* (33), 6869.
- (70) Dreiss, C. A. Wormlike Micelles: Where Do We Stand? Recent Developments, Linear Rheology and Scattering Techniques. *Soft Matter* **2007**, *3* (8), 956–970.
- (71) Burchard, W. Static and Dynamic Light Scattering from Branched Polymers and Biopolymers. *Adv. Polym. Sci.* **1983**, *48*, 1–124.
- (72) Lodge, T. P.; Han, C. C.; Akcasu, A. Z. Temperature Dependence of Dynamic Light Scattering in the Intermediate Momentum Transfer Region. *Macromolecules* **1983**, *16* (7), 1180–1183.
- (73) Doi, M.; Edwards, S. F. *The Theory of Polymer Dynamics*; Clarendon Press: 1988.
- (74) Chu, B.; Wang, Z.; Yu, J. Dynamic Light Scattering Study of Internal Motions of Polymer Coils in Dilute Solution. *Macromolecules* **1991**, *24* (26), 6832–6838.
- (75) Wu, C.; Chan, K. K.; Xia, K.-Q. Experimental Study of the Spectral Distribution of the Light Scattered from Flexible Macromolecules in Very Dilute Solution. *Macromolecules* **1995**, *28* (4), 1032–1037.
- (76) Wu, C.; Zhou, S. Internal Motions of Both Poly (N-Isopropylacrylamide) Linear Chains and Spherical Microgel Particles in Water. *Macromolecules* **1996**, *29* (5), 1574–1578.
- (77) Han, C. C.; Akcasu, A. Z. Dynamic Light Scattering of Dilute Polymer Solutions in the Nonasymptotic Q-Region. *Macromolecules* **1981**, *14* (4), 1080–1084.
- (78) Lodge, T. P. Solvent Dynamics, Local Friction, and the Viscoelastic Properties of Polymer Solutions. *J. Phys. Chem.* **1993**, *97* (8), 1480–1487.
- (79) Fytas, G.; Rizos, A.; Floudas, G.; Lodge, T. P. Solvent Mobility in Polystyrene/Aroclor Solutions by Depolarized Rayleigh Scattering. *J. Chem. Phys.* **1990**, *93* (7), 5096–5104.
- (80) Gisser, D.; Johnson, B.; Ediger, M.; von Meerwall, E. Comparison of Various Measurements of Microscopic Friction in Polymer Solutions. *Macromolecules* **1993**, *26* (3), 512–519.
- (81) Mondal, J.; Choi, E.; Yethiraj, A. Atomistic Simulations of Poly(ethylene Oxide) in Water and an Ionic Liquid at Room Temperature. *Macromolecules* **2014**, *47* (1), 438–446.
- (82) Konishi, T.; Yoshizaki, T.; Yamakawa, H. On the “Universal Constants” ρ and Φ . of Flexible Polymers. *Macromolecules* **1991**, *24* (20), 5614–5622.

(83) Mansfield, M. L.; Douglas, J. F. Shape Characteristics of Equilibrium and Non-Equilibrium Fractal Clusters. *J. Chem. Phys.* **2013**, *139* (4), 044901.

(84) Giacomelli, C.; Schmidt, V.; Borsali, R. Specific Interactions Improve the Loading Capacity of Block Copolymer Micelles in Aqueous Media. *Langmuir* **2007**, *23* (13), 6947–6955.

(85) Kikuchi, A.; Nose, T. Unimolecular-Micelle Formation of Poly(methyl Methacrylate)-Graft-Polystyrene in Iso-Amyl Acetate. *Polymer* **1996**, *37* (26), 5889–5896.

(86) Kikuchi, A.; Nose, T. Multimolecular-Micelle Formation of Poly(methyl Methacrylate)-Graft-Polystyrene in Acetonitrile/(Acetoacetic Acid Ethyl Ether). *Macromolecules* **1997**, *30* (4), 896–902.